論文 / 著書情報
Article / Book Information

Title	Corrosion behavior of Al4SiC4/SiC ceramics exposed to molten calcium-magnesium-alumino-silicate at 1350 ° C in air
Authors	Atsuko Tanaka, Anna Gubarevich, Toshiyuki Nishimura, Katsumi Yoshida
Citation	International Journal of Applied Ceramic Technology, Vol. 21, No. 4, pp. 2784-2795
Pub. date	2024, 4
DOI	https://doi.org/10.1111/ijac.14760
Creative Commons	Information is in the article.

Received: 16 October 2023 | Revised: 27 February 2024 | Accepted: 25 March 2024

DOI: 10.1111/ijac.14760

International Journal of Applied Ceramic Technology

SPECIAL ISSUE ARTICLE

Corrosion behavior of Al_4SiC_4/SiC ceramics exposed to molten calcium-magnesium-alumino-silicate at 1350°C in air

Atsuko Tanaka[1] | **Anna Gubarevich**[2] | **Toshiyuki Nishimura**[3] | **Katsumi Yoshida**[2]

[1]Department of Materials Science and Engineering, School of Materials and Chemical Technology, Tokyo Institute of Technology, Tokyo, Japan

[2]Laboratory for Zero-Carbon Energy, Institute of Innovative Research, Tokyo Institute of Technology, Tokyo, Japan

[3]Research Center for Structural Materials, National Institute for Materials Science, Tsukuba, Japan

Correspondence
Atsuko Tanaka, Department of Materials Science and Engineering, School of Materials and Chemical Technology, Tokyo Institute of Technology, 2-12-1, Ookayama, Meguro-ku, Tokyo, 152–8550 Japan.
Email: tanaka.a.aw@m.titech.ac.jp

Funding information
Tokyo Institute of Technology, Japan

Abstract

Al_4SiC_4 shows excellent heat resistance, thermal shock resistance, machinability, and oxidation resistance. We focused on Al_4SiC_4-based ceramics with SiC as a non-oxide matrix for ceramic matrix composites for aircraft jet engines. In this study, monolithic Al_4SiC_4 and Al_4SiC_4/SiC ceramics were fabricated by hot-pressing, and a corrosion test against molten calcium-magnesium-alumino-silicate (CMAS) was conducted at 1350°C for 12–100 h in air, and their corrosion behavior was investigated. Scanning electron microscopy and energy-dispersive X-ray spectroscopy results revealed that severe damage was not observed at the interface between CMAS and the samples after the CMAS corrosion test. The recession of Al_4SiC_4-100, -10, and SiC-100 after corrosion for 100 h was 80–90 μm, and that of Al_4SiC_4-50 was the highest of all samples and the value was 130 μm. The dissolution behavior of the oxidation layer into molten CMAS via a corrosion reaction was dependent on the composition of both the sample and the oxidation layer, the thickness, and the microstructure of the oxidation layers. The dominant mechanism of reaction between CMAS and Al_4SiC_4-100, -90, and -50 samples was concluded to be the dissolution of the oxidation products, while in SiC-100 and Al_4SiC_4-10 samples, the dominant reaction was determined to be direct corrosion of the surface with CMAS.

KEYWORDS
aluminum silicon carbide, corrosion/corrosion resistance, oxidation, silicon carbide

1 | INTRODUCTION

SiC fiber-reinforced SiC (SiC_f/SiC) composites are one of the representative ceramics matrix composites (CMC), and they have been recognized as the next generation highly reliable heat resistant materials.[1,2] CMC have light weight and excellent heat resistance rather than metals and show pseudo-ductile fracture behavior with complicated fracture process, resulting in showing damage tolerance.[2–4] SiC_f/SiC composites have been expected to be applied as

hot components for aircraft jet engines.[4–8] When CMC is used for jet engine components in actual environments, dry- and wet-oxidation and corrosion resistance against volcanic ash and sand at high temperatures are strongly required in addition to excellent thermal and mechanical properties.[7–10]

To prevent dry- and wet-oxidation and corrosion with molten calcium-magnesium-alumino-silicate (CMAS), the main chemical components of volcanic ash and sand, CMC used for aircraft jet engines are commonly covered with environmental barrier coating (EBC).[7–11] To date, many kinds of materials have been studied for use as EBCs. Materials such as yttria-stabilized zirconia (YSZ), $Gd_2Zr_2O_7$, $Yb_2Si_2O_7$, and Gd_2SiO_5 have been studied for use as an EBC because these materials react with molten CMAS and rare-earth-apatite phases are rapidly formed to minimize the damage to CMAS penetration.[12–15] However, when EBC is damaged or peeled off, the environmental resistance deteriorates, and the safety and reliability of the jet engine components cannot be maintained. Furthermore, the complicated fabrication process of CMC combined with the EBC formation process makes the fabrication process more complex and causes high production costs. To enhance the resistance to environmental effects, the CMC can be developed with a matrix that has excellent oxidation and corrosion resistance, which would result in lower production costs and improved reliability.

The present authors have paid attention to the nanolayered-ternary compounds, which show unique characteristics and properties of both ceramics and metals such as excellent corrosion resistance, heat resistance, thermal shock resistance, and machinability.[16,17] Aluminum silicon carbide, Al_4SiC_4, one of the nanolayered-ternary compounds, has high oxidation and corrosion resistance due to the formation of protective layers by oxidation at high temperatures.[18-22] In addition, Lee et al. fabricated SiC ceramics with Al_4SiC_4 as a sintering additive by hot-pressing at 1700°C, and it is suggested that Al_4SiC_4 is effective in densifying SiC ceramics.[23] Thus, we focused on Al_4SiC_4/SiC ceramics.

Considering the application of CMC for aircraft jet engines, understanding the basic oxidation and CMAS corrosion behavior of Al_4SiC_4-based ceramics in air at high temperatures becomes one of the important studies. With regard to the oxidation of monolithic Al_4SiC_4, Inoue et al. reported that monolithic Al_4SiC_4 ceramics after oxidation at 1500°C for 10 h consisted of the layered structure with different compositions such as SiC, Al_2O_3, and $3Al_2O_3{\cdot}2SiO_2$ (mullite).[24] In our previous study, Al_4SiC_4-based ceramics with SiC were fabricated by hot-pressing at 1800°C, and their oxidation behavior at 1350°C in dry air was investigated.[25] It has been reported that Al_4SiC_4/SiC ceramics after oxidation at 1350°C consisted of the oxidation layers with SiO_2/SiC, mullite, and Al_2O_3, and the number of the oxidation layers tended to increase with Al_4SiC_4 content and the oxidation time. Furthermore, the thickness of the oxidation layer change and the weight change obeyed parabolic rate law.[25] However, there are very few reports on the corrosion behavior against molten CMAS of monolithic Al_4SiC_4, monolithic SiC, and Al_4SiC_4/SiC ceramics at high temperatures in air. In this study, monolithic Al_4SiC_4 and Al_4SiC_4/SiC ceramics were fabricated by hot-pressing, and a corrosion test against molten CMAS was conducted at 1350°C for 12–100 h in air, and their corrosion behavior against molten CMAS was investigated. In this study, the temperature for the corrosion test was set as 1350°C by considering the expected operation temperature (material surface temperature) for hot components of aircraft jet engines in the range of 1300–1400°C.[26]

TABLE 1 The composition of Al_4SiC_4/SiC ceramics and their relative density and open porosity.

Sample name	Al_4SiC_4 (vol %)	SiC (vol %)	Relative density (%)	Open porosity (%)
Al_4SiC_4-100	100	0	91.0	0.30
Al_4SiC_4-90	90	10	94.3	0.30
Al_4SiC_4-50	50	50	93.2	0.38
Al_4SiC_4-10	10	90	87.4	3.91
SiC-100	0	100	98.4	0.16

2 | EXPERIMENTAL PROCEDURES

2.1 | Preparation of Al_4SiC_4-based ceramics by hot-pressing

According to our previous study,[25] monolithic Al_4SiC_4 and Al_4SiC_4/SiC ceramics were fabricated by hot-pressing at 1800°C for 2 h in Ar flow at mechanical pressure of 40 MPa using Al_4SiC_4 powder (D50: 3.3 μm, Tateho Chemical Industries Co., Ltd.) and β-SiC powder (D50: 0.5 μm, Höganäs) as the starting powders. The volume ratio of Al_4SiC_4 to SiC was 100:0 (denoted as Al_4SiC_4-100), 90:10 (Al_4SiC_4-90), 50:50 (Al_4SiC_4-50), and 10:90 (Al_4SiC_4-10). For comparison with Al_4SiC_4-based ceramics, commercially available α-SiC (Kyocera Corporation; denoted as SiC-100) was used. Table 1 shows their relative density and open porosity measured by Archimedes' method. Their relative density was calculated using the theoretical density of Al_4SiC_4 and SiC, which was 3.03 and 3.21 g/cm^3, respectively.[19,27] The samples were almost fully densified under the present hot-pressing condition, and their relative density was higher than 90% except for Al_4SiC_4-10.

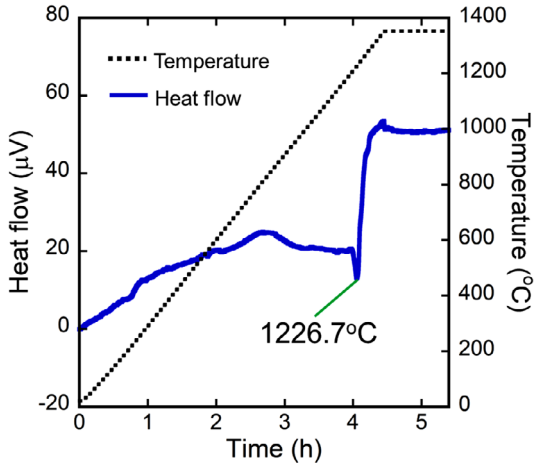

FIGURE 1 DTA curve of calcium-magnesium-alumino-silicate (CMAS) powder from room temperature to 1350°C in air.

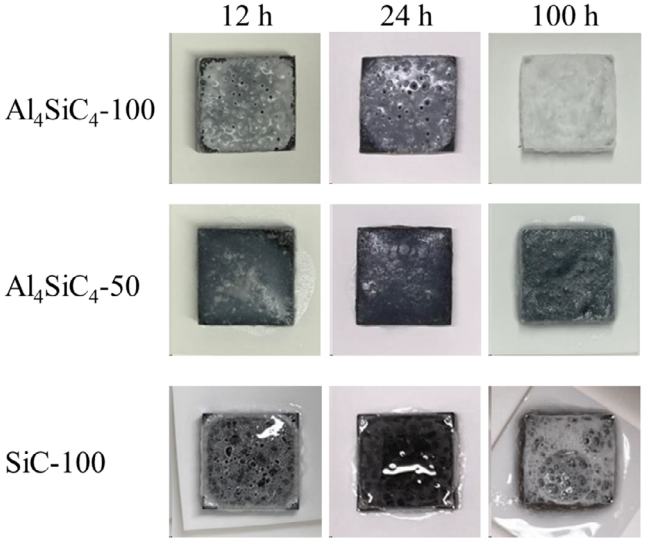

FIGURE 2 The appearance of the samples after the calcium-magnesium-alumino-silicate (CMAS) corrosion test.

2.2 | Preparation of CMAS powder

CMAS powder was synthesized using CaO (Kanto Chemical Co., Inc.), MgO (Iwatani Chemical Industry Co., Ltd.), α-Al_2O_3 (Taimei Chemicals Co., Ltd.), and SiO_2 (Quartz, FUJIFILM Wako Pure Chemical Corporation) as the starting powders. The starting powders were mixed at the molar ratio of 25CaO-14.5MgO-10.5Al_2O_3-50SiO_2. Many researchers have been studying the corrosion behavior of materials against CMAS with various compositions. The amount of Ca in CMAS has been reported to affect corrosion, and the effect of Ca on the corrosion behavior is often discussed in terms of the Ca/Si ratio.[11,28] In this study, a Ca/Si molar ratio of 0.5 was used to achieve a melting point below 1350°C and was within the values of 0.4–1.7, as reported by Levi et al.[29] According to the phase diagram,[30] the composition of CMAS was determined to be 25CaO-14.5MgO-10.5Al_2O_3-50SiO_2. CMAS powder was synthesized by heat treatment at 1200°C for 24 h in air, followed by finely grinding using SiC mortar and pestle. To confirm the melting point of the synthesized CMAS powder, thermogravimetry and differential thermal analysis (TG-DTA; 2020SA, Bruker AXS K. K.) were conducted, and the CMAS powder was confirmed to be melted around 1230°C as shown in Figure 1.

2.3 | Corrosion test with molten CMAS and characterization of corroded samples

The hot-pressed Al_4SiC_4-based ceramics were cut into the plates with the size of 15 × 15 × 3 mm^3 and their surface was mirror-polished using 1 μm diamond slurry. CMAS pellets were formed using about 0.25 g of synthesized CMAS powder in a mold (ϕ10) by uniaxial pressing at the pressure of 470 MPa. The CMAS pellet was placed on the top surface of the samples, and the sample with the CMAS pellet was placed in an Al_2O_3 crucible in an air furnace. The thermocouple (B-type in JIS, Pt-Rh30%) was located near the Al_2O_3 crucible, and the temperature near the sample was measured. CMAS corrosion test was conducted at 1350°C for 12, 24, and 100 h in air. The appearance of the samples after the CMAS corrosion test is shown in Figure 2. After the corrosion test, the appearance of molten CMAS on SiC-100, Al_4SiC_4-50, and Al_4SiC_4-100 was transparent, translucent, and opaque, respectively. Molten CMAS spread widely on the surface of the samples, and the present experiment had the validity to confirm the reaction of the samples against molten CMAS. After the CMAS corrosion test, the corroded surface of the samples was covered with resin, and then the specimens were cut and their cross-section was mirror-polished with 1 μm diamond slurry. Polished specimens were observed with a scanning electron microscope (SEM, JSM-700, JEOL Ltd., and S-4800H, HITACHI, accelerating voltage: 15 kV) to evaluate microstructural change and the reaction layer of the corroded specimens with molten CMAS. Elemental distribution of the specimens after the CMAS corrosion test was analyzed with an energy-dispersive X-ray spectroscope (EDS, accelerating voltage: 5 kV) equipped with SEM. The crystalline phases of the samples after the corrosion test were analyzed by X-ray diffractometry (XRD, Aeris; Malvern Panalytical Ltd.). The recession of the samples after the CMAS corrosion test was roughly estimated by optical microscopy (ECLIPSE LV100ND, Nikon Corp.).

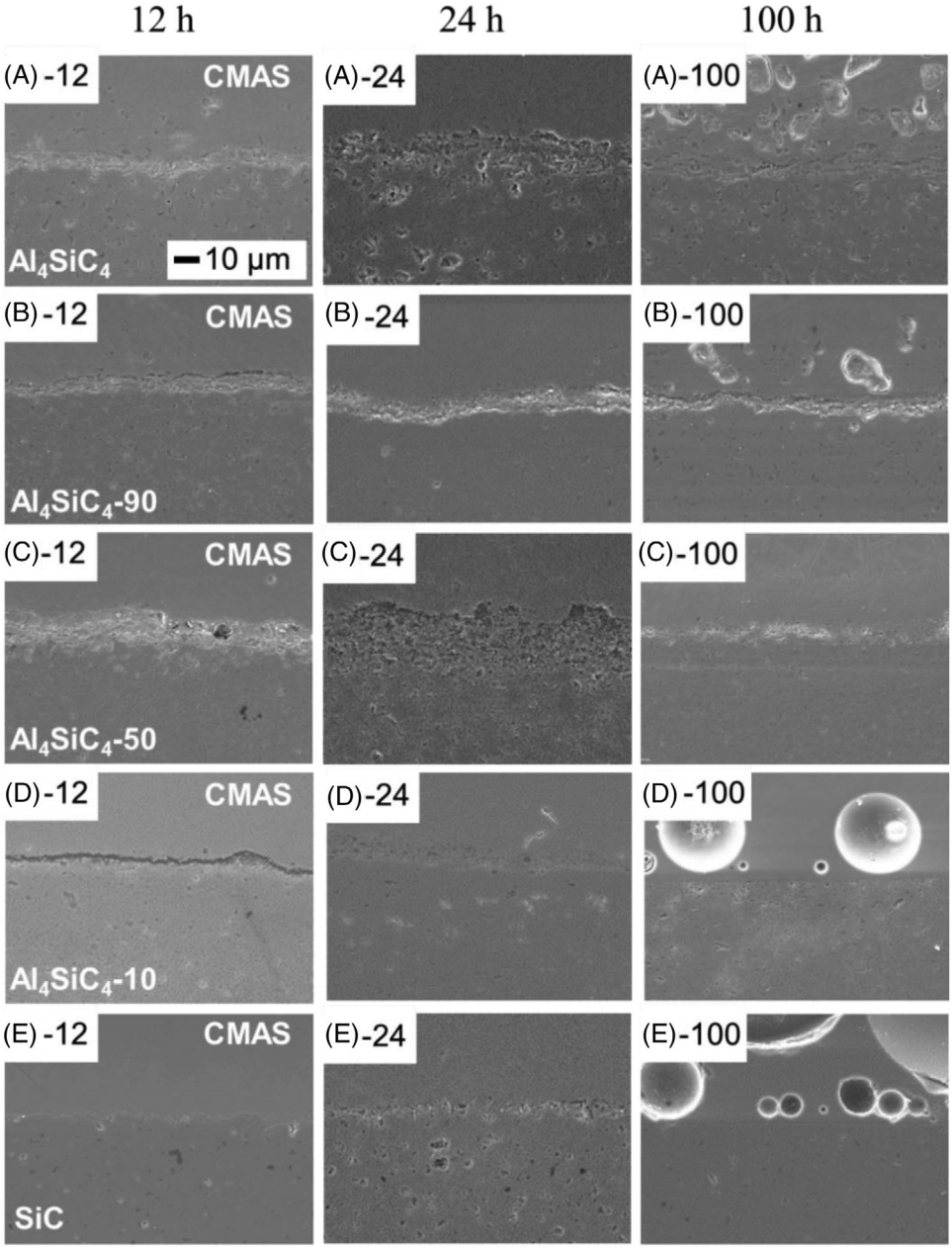

FIGURE 3 Cross-sectional SEM images of the samples after the calcium-magnesium-alumino-silicate (CMAS) corrosion test at 1350°C for 12–100 h in air. (A) Al_4SiC_4-100, (B) Al_4SiC_4-90, (C) Al_4SiC_4-50, (D) Al_4SiC_4-10, and (E) SiC-100. The number after the alphabetical sample code represents corrosion time (hours).

3 | RESULTS

3.1 | SEM observation of Al_4SiC_4, SiC, and Al_4SiC_4/SiC ceramics after CMAS corrosion test at 1350°C and their reaction layer thickness

Figure 3 shows the cross-sectional SEM images of the samples after the CMAS corrosion test at 1350°C for 12–100 h in air. Damaged layers were clearly observed in SEM images of the samples after the CMAS corrosion test. Damaged layers for all the samples were formed after the corrosion test, and some parts of the damaged layer were porous. The thickness of damaged layers was measured at five points or more in the region of 120–360 μm of SEM images, and the average thickness was calculated. The average thickness of the damaged layers is shown in Figure 4.

The damaged layer in SiC-100 was extremely thin regardless of corrosion time. Whereas the thickness of the damaged layer of SiC-100 corroded for 12 h was less than 1 μm, that for 24 h was around 5 μm. However, the thickness

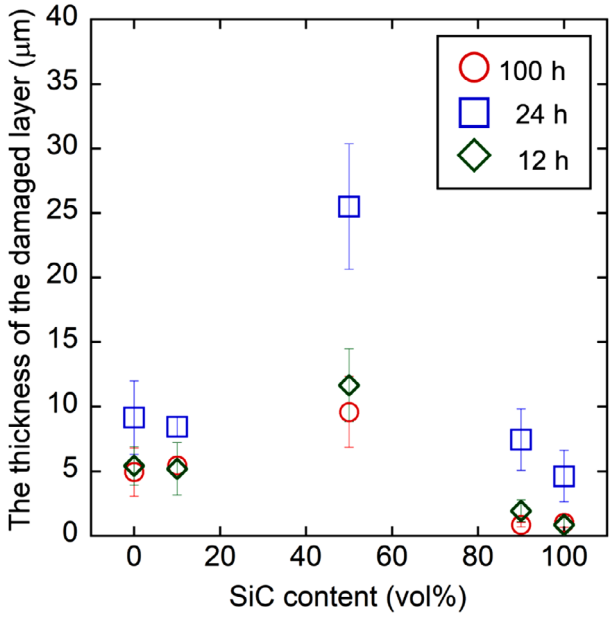

FIGURE 4 The average thickness of the damaged layers of the sample after the calcium-magnesium-alumino-silicate (CMAS) corrosion test. The bar for each plot shows the standard deviation of the damaged layer thickness.

of the damaged layer of SiC-100 corroded for 100 h was reduced to less than 1 μm. The thickness of the damaged layer of Al_4SiC_4-10 after the corrosion test for 12 and 100 h was very thin as well as SiC-100, which for 24 h was as thick as 7 μm.

In the case of Al_4SiC_4-100, -90, and -50, the thickness of their damaged layer increased with CMAS corrosion time up to 24 h, and that was decreased after CMAS corrosion for 100 h as well as Al_4SiC_4-10 and SiC-100. The thickness of the damaged layer of Al_4SiC_4-50 after the CMAS corrosion test for 24 h was around 25 μm and this value was the thickest of all samples under the present experimental condition. The interface between molten CMAS and the Al_4SiC_4-100, -90, and -50 after the corrosion test for 24 h was slightly rough rather than that of 12 h. The interface of CMAS and samples after CMAS corrosion for 100 h was relatively flat, and the samples seemed to be corroded uniformly.

3.2 | EDS analysis of the cross-section of Al_4SiC_4-based ceramics after CMAS corrosion test at 1350°C

Figure 5 shows the EDS analysis (point analysis) of Al_4SiC_4-100 after the CMAS corrosion test of 1350°C for 100 h. The regions I, II, and III correspond to the inside of the CMAS, the damaged layer, and the sample, respectively. Ca and Mg were detected in the CMAS region (Figure 5(I)), whereas they were not detected in the damaged layer (Figure 5(II)) and Al_4SiC_4-100 (Figure 5(III)). Ca and Mg were not detected in the region III of other samples. These results suggested that Ca and Mg did not diffuse into the samples, and they did not contribute to the corrosion of the samples. Therefore, the EDS mappings of Ca and Mg were excluded from the following explanation of the results regarding EDS mapping.

The cross-sectional EDS mapping of the samples after the CMAS corrosion test was exhibited in Figure 6 and Figure S1. As observed in SEM images, severe damage was not observed at the interface between CMAS and samples, and there was no corrosion caused by the penetration of CMAS, and this result differed from the candidate materials such as $Y_2Si_2O_7$ and $Gd_2Zr_2O_7$ for EBC that form apatite phases by CMAS corrosion.[12–15] In other words, the Al_4SiC_4-based samples fabricated in this study did not form an apatite phase.

The thickness of the damaged layers observed in SEM images almost corresponded to the thickness of the reaction layers in EDS mappings. Hereafter, the damaged layer was denoted as the reaction layer.

In SiC-100, SEM observation revealed that the reaction layer was very thin, the region corresponding to the reaction layer was not detected by EDS, and the interface between CMAS and SiC-100 after CMAS corrosion for 100 h was smooth rather than for 12 and 24 h. In the case of Al_4SiC_4-100, the region corresponding to the reaction layer observed by SEM mainly contained carbon (C), and the reaction layer after the corrosion test for 12 h had the structure consisting of regions with high Al/O content and high Si/C content. As well as Al_4SiC_4-100, Al_4SiC_4-90 had the reaction layer containing C, and Si and Al were observed in the whole area of the EDS mapping, and Si and Al existed with C in the reaction layer. In the case of the EDS mapping of Al_4SiC_4-50, the reaction layer observed in SEM images mainly contained C. Under the present experimental condition, although this reaction layer became thick when Al_4SiC_4-50 was corroded with molten CMAS for 24 h, its thickness became thin after CMAS corrosion for 100 h. In addition, Al was not detected in this region, and the distribution of Si gradually reduced from the bottom of the reaction layer to the interface between CMAS and the reaction layer for the Al_4SiC_4-50 corroded for 24 h. In the case of Al_4SiC_4-10 after corroding for 12 and 24 h, the thickness of the reaction layer observed in SEM images was in agreement with the thickness of the C region in EDS mapping. As the reaction layer of Al_4SiC_4-10 corroded for 100 h was very thin in the SEM image as well as SiC-100, the region corresponding to the reaction layer was not observed in EDS mapping.

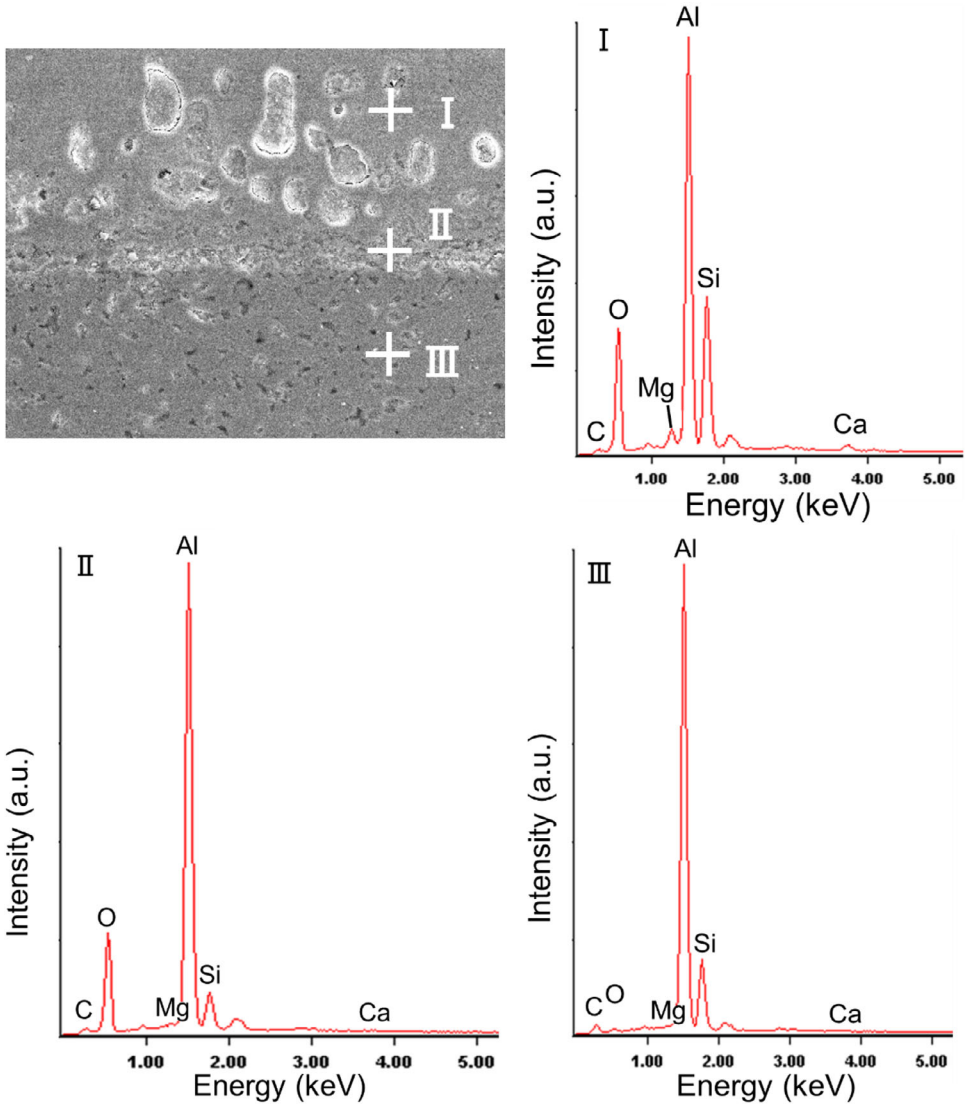

FIGURE 5 Energy-dispersive X-ray spectroscope (EDS) analysis (point analysis) of Al_4SiC_4-100 after calcium-magnesium-alumino-silicate (CMAS) corrosion test at 1350°C for 100 h in (I) CMAS region, (II) reaction layer, and (III) Al_4SiC_4-100.

3.3 | Reaction products of Al_4SiC_4-based ceramics after corrosion test with CMAS analyzed by XRD

In order to identify the crystalline and non-crystalline phases of the reaction layer by XRD, the CMAS-adhered samples were gradually polished from the CMAS to the region around the interface between CMAS and the sample until the diffraction peaks derived from CMAS disappeared as shown in Figure 7. CMAS region and the region around the interface between CMAS and the sample were analyzed, and the crystalline and non-crystalline phases of the samples after the CMAS corrosion test for 100 h were listed in Table 2. The major phases in Table 2 were underlined, and original crystalline phases derived from as-prepared samples are excluded from this table.

The composition of synthesized CMAS was decided based on the composition of 58 mol% anorthite ($CaAl_2Si_2O_8$) and 42 mol% diopside ($CaMgSi_2O_6$), and its melting point is lower than 1350°C. The synthesized CMAS powder at 1200°C consisted of anorthite, diopside, and quartz. The synthesized CMAS became amorphous after melting at 1350°C and the residual CMAS on Al_4SiC_4-10 and SiC-100 after the CMAS corrosion test was also amorphous. On the contrary, the residual CMAS on Al_4SiC_4-100, -90, and -50 after the CMAS corrosion test mainly contained anorthite, and the phases in the residual CMAS changed with the sample composition.

The present authors reported that mullite, Al_2O_3, and SiO_2 (cristobalite) were formed in Al_4SiC_4-100 as oxidation products after the oxidation test without CMAS, and SiC was also formed by the following oxidation reaction[25];

$$Al_4SiC_4(s) + 6O_2(g) \rightarrow 2Al_2O_3(s) + SiC(s) + 3CO_2(g)$$

$$Al_4SiC_4(s) + 3O_2(g) \rightarrow 2Al_2O_3(s) + SiC(s) + 3C(s)$$

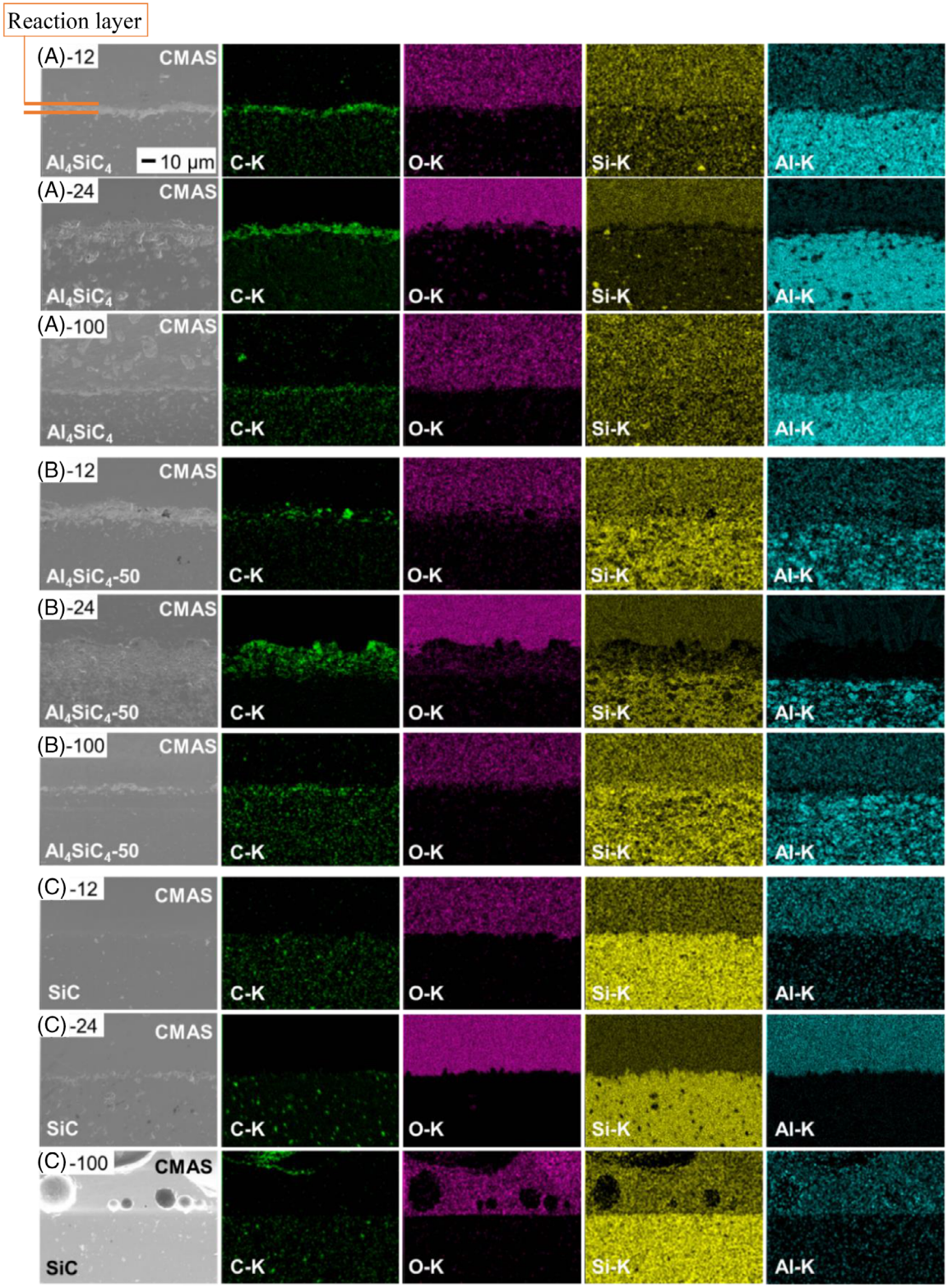

FIGURE 6 Energy-dispersive X-ray spectroscope (EDS) mappings of the cross-section of (A) Al_4SiC_4-100, (B) Al_4SiC_4-50, and (C) SiC-100 after calcium-magnesium-alumino-silicate (CMAS) corrosion test at 1350°C for 12–100 h in air. The number after the alphabetical sample code represents corrosion time (hours).

TABLE 2 The crystalline and amorphous phases of the samples after the calcium-magnesium-alumino-silicate (CMAS) corrosion test at 1350°C for 100 h analyzed by X-ray diffractometry (XRD).

	Al_4SiC_4-100	Al_4SiC_4-90	Al_4SiC_4-50	Al_4SiC_4-10	SiC-100
CMAS region	Anorthite Spinel Mullite α-Al_2O_3 α-SiC Cristobalite Quartz	Anorthite Mullite Cristobalite	Anorthite Diopside Mullite α-Al_2O_3 Cristobalite Al_4O_4C Spinel Quartz	Amorphous	Amorphous
The region around the interface between CMAS and the sample	Mullite Al_4O_4C α-SiC	Mullite α-Al_2O_3 Al_4O_4C Spinel Quartz	α-Al_2O_3 Al_4O_4C	α-Al_2O_3 Mullite Cristobalite Spinel Diopside	Cristobalite α-Al_2O_3 Mullite Spinel Diopside Quartz Carbon

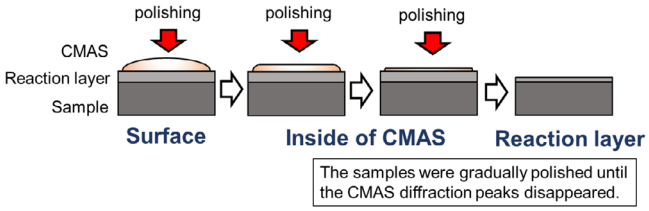

FIGURE 7 Schematic illustration of polishing procedures of the calcium-magnesium-alumino-silicate (CMAS)-adhered samples after CMAS corrosion test for X-ray diffractometry (XRD) analysis.

In the present result of Al_4SiC_4-100, the CMAS region and the interface between CMAS and the sample contained mullite, Al_2O_3, SiO_2 (cristobalite), and SiC. Mullite and Al_2O_3 were the main products after the CMAS corrosion test, except for anorthite, the crystalline phase of CMAS. In addition, Al_2O_3 and SiO_2 (cristobalite) existed in the CMAS region. These oxides formed as the oxidation products on Al_4SiC_4-100 would be dissolved into molten CMAS. These oxides were detected in the CMAS region due to the rough interface between the sample and molten CMAS. In the case of Al_4SiC_4-90, mullite was a major phase (around 50 wt%) in the CMAS region except for anorthite, and mullite and Al_2O_3 were detected at the interface between CMAS and the sample. In the case of Al_4SiC_4-50, mullite and Al_2O_3 were detected in the CMAS region as well as Al_4SiC_4-100, and Al_2O_3 was detected at the interface between CMAS and the sample. Furthermore, Al_4O_4C and spinel and SiO_2 (cristobalite) could also form as minor phases in Al_4SiC_4-100, -90, and -50.

All the reaction products in Al_4SiC_4-10 and SiC-100 would exist in the region around the interface between CMAS and the sample because the residual CMAS on

TABLE 3 The recession of the samples after the calcium-magnesium-alumino-silicate (CMAS) corrosion test at 1350°C for 12, 24, and 100 h.

	CMAS corrosion time at 1350°C		
	12 h	24 h	100 h
Sample name	The recession of the sample (μm)		
Al_4SiC_4-100	20	30	90
Al_4SiC_4-90	0	10	110
Al_4SiC_4-50	0	20	130
Al_4SiC_4-10	20	50	90
SiC-100	10	40	80

Al_4SiC_4-10 and SiC-100 after the CMAS corrosion test was amorphous, and anorthite was not detected. The products around the interface between the CMAS region and Al_4SiC_4-10 formed by the CMAS corrosion test were the same as those in other samples containing Al_4SiC_4. As for SiC-100, a small amount of Al_2O_3 and mullite were formed, but SiO_2 (cristobalite), an oxidation product of SiC, was formed by the CMAS corrosion test. The CMAS corrosion mechanism based on the dissolution of the oxidation layer into CMAS on the samples was discussed in section 4.

3.4 | Recession of Al_4SiC_4-based ceramics after CMAS corrosion test

Figure 8 and Table 3 show the change in the recession (reduction thickness) with CMAS corrosion time roughly estimated by optical microscopy. The recession of all samples was approximately linearly increased with corrosion time. As for all samples after CMAS corrosion for 100 h,

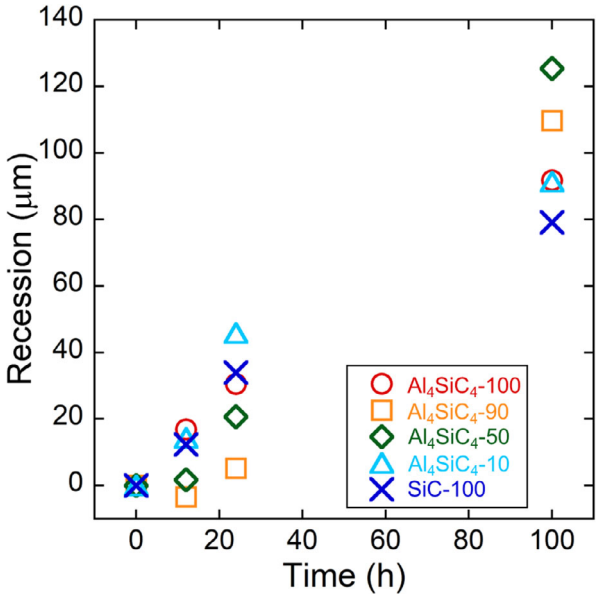

FIGURE 8 The change in the recession of the samples with calcium-magnesium-alumino-silicate (CMAS) corrosion time.

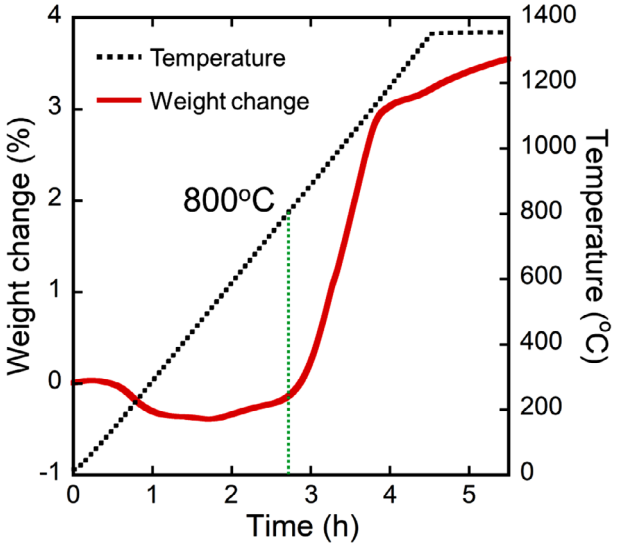

FIGURE 9 Thermogravimetry (TG) curve of Al_4SiC_4-100 from room temperature to 1350°C in air.

their recession ranged from 80 to 130 μm, and the recession proceeded by the reaction with molten CMAS. The recession of SiC-100, Al_4SiC_4-10, and −100 was almost the same as 80–90 μm, and that of Al_4SiC_4-50 was 130 μm and this value was the highest under the experimental condition in the present study.

4 | DISCUSSION

First, the corrosion behavior of Al_4SiC_4/SiC ceramics against molten CMAS at 1350°C was discussed based on their oxidation behavior. Figure 9 shows the TG curve of Al_4SiC_4-100 from room temperature to 1350°C in air. The TG curve of Al_4SiC_4-100 showed a small weight loss up to around 600°C, and then the weight drastically increased from around 800°C. Above 1150°C, the weight gradually increased. Yamamoto et al. reported that the marked mass gain by oxidation of Al_4SiC_4 was observed with the formation of Al_2O_3 and SiO_2 in the temperature range of 850–1150°C, and the weight slightly increased above 1150°C.[31] This oxidation reaction agreed with our result (Figure 9), and the oxidation of Al_4SiC_4-100 started from 800°C. DTA result in Figure 1 suggested that CMAS melted around 1230°C. This means that firstly the oxidation of the samples containing Al_4SiC_4 occurred followed by the melting of CMAS, resulting in taking place the reaction between the oxidation layer and molten CMAS. DTA experiment was conducted to confirm the chemical reaction between oxides and Al_4SiC_4/SiC at the temperature below the melting point of CMAS. Al_4SiC_4/SiC with CMAS powder was heated up to 1220°C without holding time in TG-DTA. As a result, it was confirmed that Al_4SiC_4 formed some oxides on its surface by its oxidation, but CMAS powder did not melt and did not react with Al_4SiC_4.

As described in the introduction, the results in the previous oxidation test indicated that Al_4SiC_4/SiC ceramics after oxidation at 1350°C consisted of oxidation layers with SiO_2/SiC, mullite, and Al_2O_3, and the number of the oxidation layers tended to increase with Al_4SiC_4 content and the oxidation time.

Based on the results described above, the reaction layer thickness of the sample after the CMAS corrosion test was discussed to be compared with the oxidation layer thickness formed by the oxidation test. Hereafter, the reaction layers have been distinguished from each other and named four kinds of layers; “the oxidation layer” is in our previous oxidation test, “the corroded layer” is formed by the reaction with the samples and the oxides in CMAS during CMAS corrosion test, “initial oxidation layer” is formed by initial oxidation below CMAS melting point and “residual oxidation layer” is residual “initial oxidation layer” after corrosion by CMAS.

There are two possible corrosion reactions between molten CMAS and the samples; (1) oxidation products on the samples formed by oxidation dissolve into molten CMAS, and (2) molten CMAS corrodes the sample directly and a corroded layer is formed. EDS mapping of the reaction layer in Al_4SiC_4-100 after CMAS corrosion test for 12 and 24 h showed the region with higher Al/O (Al_2O_3) content and higher Si/C (SiC) content and this composition in the reaction layer was different from that in the oxidation layer observed after oxidation test without CMAS. These results suggested that the oxidation layer would dissolve into molten CMAS, the oxidation layer still remains as the residual oxidation layer, and the dissolution of the

oxidation layer into molten CMAS could be dominant. Furthermore, XRD results indicated that the composition of molten CMAS was changed after the corrosion test, and the results supported the dissolution of the reaction layer on the sample surface into molten CMAS. On the other hand, in SiC-100 and Al_4SiC_4-10, the corrosion of the samples with molten CMAS could be dominant because of the following reasons; (1) the oxidation layer thickness of these samples observed in the oxidation test without CMAS was very thin, (2) the region corresponding to the reaction layer was not observed by EDS, and (3) the recession of SiC-100 and Al_4SiC_4-10 after CMAS corrosion test for 100 h was around 80 and 90 μm, respectively.

In order to discuss and confirm the chemical compositional change of CMAS and the dissolution of the samples into molten CMAS, the following experiment was conducted; the synthesized CMAS powder was once melted at 1350°C for 12 h, and the CMAS powder was crushed into the powder. Subsequently, 5 mol% Al_2O_3, mullite, or SiO_2 were added to the CMAS powder, and the melting point of the CMAS with each oxide was measured by TG-DTA and phases formed after heating in CMAS at 1350°C for 12 h was identified by XRD. While as-synthesized CMAS powder melted at 1227°C, CMAS powder mixed with 5 mol% Al_2O_3, mullite, and SiO_2 melted at 1210, 1203, and 1200°C, respectively, and the melting point of CMAS mixed with SiO_2 became lower than that of others. With regard to phases formed after heating at 1350°C, CMAS with 5 mol% SiO_2 addition became amorphous as well as the synthesized CMAS after melting. The phase of CMAS with 5 mol% Al_2O_3 or 5 mol% mullite addition after melting was anorthite, and its content was around 80 wt%. This result also suggested that Al_2O_3 and mullite, which contain Al, would promote the change of crystalline phases of molten CMAS. The crystalline phases of the residual CMAS on Al_4SiC_4-100, -90, and -50 after the CMAS corrosion test were anorthite, and that on Al_4SiC_4-10 and SiC-100 after the CMAS corrosion test was amorphous. These results would be reasonable. It is revealed that the oxidation layers such as Al_2O_3, mullite, and SiO_2, of the samples could dissolve into CMAS, and the composition of CMAS was changed. According to the ternary phase diagram of anorthite, diopside, and quartz, the ternary eutectic composition is 30 wt% quartz, 33 wt% diopside, and 37 wt% anorthite at 1200°C,[32] and it suggests that the reaction of SiO_2 into synthesized CMAS makes its melting point lower. As the melting point of CMAS becomes lower, the samples with oxidation layers would contact molten CMAS for a longer time, resulting in possibly promoting the dissolution of oxidation layers into molten CMAS.

Then, the reason why the recession of Al_4SiC_4-50 after CMAS corrosion for 100 h became the highest was discussed based on the reaction layer and the recession. In the oxidation test in our previous study, whereas the Al_2O_3 layer in Al_4SiC_4-100 was as thick as the SiO_2 layer containing SiC, the SiO_2/SiC layer containing Al_4SiC_4 in Al_4SiC_4-50 was much thicker than Al_2O_3 layer, and it suggested that the oxidation layer of Al_4SiC_4-50 had high SiO_2 content. In addition, initially, SiC in Al_4SiC_4-50 and SiC formed by the oxidation of Al_4SiC_4 would be present in the sample at 1350°C in air, and those SiC was oxidized to the SiO_2. Thus, the SiO_2/SiC layer of Al_4SiC_4-50 would become much thicker than the Al_2O_3 layer, resulting in high SiO_2 content in the oxidation layer of Al_4SiC_4-50. Besides, the residual reaction layer after the CMAS corrosion test contained Si/O/C (SiO_2/SiC), and the layer was porous as seen in the SEM images (Figure 3), and the porous layer was assumed to be dissolved easily into molten CMAS due to its higher surface area.

From these results, the dissolution behavior of the oxidation layers into molten CMAS was considered to depend on the composition of both the sample and the oxidation layer, the thickness, and the microstructure of the oxidation layer. In consideration of the reactions between the molten CMAS and the sample under the present experimental conditions, the dissolution of the oxidation products on the samples into molten CMAS could be the dominant mechanism in Al_4SiC_4-100, -90, and -50, and the direct corrosion of the samples with molten CMAS could be dominant mechanism in SiC-100 and Al_4SiC_4-10.

It is concluded that Al_4SiC_4/SiC ceramics are expected to be one of the promising materials as a novel non-oxide matrix for CMC as an alternative material to SiC.

5 | CONCLUSION

The corrosion test of monolithic Al_4SiC_4 and Al_4SiC_4/SiC ceramics against molten CMAS was conducted at 1350°C for 12–100 h in air, and their corrosion behavior was investigated.

From the SEM and EDS results, severe damage was not observed at the interface between CMAS and the samples. The recession of all samples was approximately linearly increased with corrosion time. The recession of Al_4SiC_4-100, -10, and SiC-100 after corrosion for 100 h was almost the same as 80–90 μm, and that of Al_4SiC_4-50 was the highest of all samples and the value was 130 μm. The dissolution behavior of the oxidation layer into molten CMAS as a corrosion reaction was considered to depend on the composition of both the sample and the oxidation layer, the thickness, and the microstructure of the oxidation layer. Based on these results, the dominant mechanism of reaction between the molten CMAS and the Al_4SiC_4-100, -90, and -50 samples was concluded to be the dissolution of the oxidation products, while in the SiC-100 and

Al_4SiC_4-10 samples, the dominant reaction was determined to be direct corrosion of the surface with molten CMAS. It is concluded that Al_4SiC_4/SiC ceramics are expected to be one of the promising materials as a novel non-oxide matrix for CMC as an alternative material to SiC.

ACKNOWLEDGMENTS

The authors would like to deeply appreciate Dr. Shintaro Yasui and Dr. Ayumi Itoh (Tokyo Institute of Technology, Japan) for their kind support in conducting SEM observation and EDS analysis.

ORCID

Atsuko Tanaka https://orcid.org/0009-0007-1400-3893
Anna Gubarevich https://orcid.org/0000-0003-4959-0227
Katsumi Yoshida https://orcid.org/0000-0002-2735-2263

REFERENCES

1. Naslain RR, Pailler RJF, Lamon JL. Single- and multilayered interphases in SiC/SiC composites exposed to severe environmental conditions: an overview. Int J Appl Ceram Technol. 2010;7(3):263–75.
2. Ruggles-Wrenn M, Boucher N, Przybyla C. Fatigue of three advanced SiC/SiC ceramic matrix composites at 1200°C in air and in steam. Int J Appl Ceram Technol. 2018;15:3–15.
3. Kaya H. The application of ceramic–matrix composites to the automotive ceramic gas turbine. Compos Sci Technol. 1999;59:861–72.
4. Spitsberg I, Steibel J. Thermal and environmental barrier coatings for SiC/SiC CMCs in aircraft engine applications. Int J Appl Ceram Technol. 2004;1(4):291–301.
5. Aoki T, Ogasawara T, Okubo Y, Yoshida K, Yano T. Fabrication and properties of Si—Hf alloy melt-infiltrated Tyranno ZMI fiber/SiC-based matrix composites. Compos Part A Appl Sci Manuf. 2014;66:155–62.
6. Steibel J. Ceramic matrix composites taking flight at GE Aviation. Am Ceram Soc Bull. 2019;98:30–33.
7. Arai Y, Aoki Y, Kagawa Y. Effect of cristobalite formation on the delamination resistance of an oxide/Si/(SiC/SiC) environmental barrier coating system after cyclic high temperature thermal exposure. Scr Mater. 2017;139:58–62.
8. Lee KN, Roode MV. Environmental barrier coatings enhance performance of SiC/SiC ceramic matrix composites. Am Ceram Soc Bull. 2019;98:46–53.
9. Tanaka M, Kitaoka S, Yoshida M, Sakurada O, Hasegawa M, Nishioka K, et al. Structural stabilization of EBC with thermal energy reflection at high temperatures. J Euro Ceram Soc. 2017;37:4155–61.
10. Lee KN. Environmental barrier coatings for SiC_f/SiC. In: Bansal NP, Lamon J, editors. Ceramic matrix composites: materials, modeling and technology. 1st ed. Hoboken, NJ: John Wiley & Sons Inc.; 2015:430–51.
11. Xiao S, Li J, Huang P, Zhang A, Tian Y, Zhang X, et al. Evaluation of environmental barrier coatings: A review. Int J Appl Ceram Technol. 2023;20:2055–76.
12. Wu J, Guo H, Gao Y, Gong S. Microstructure and thermophysical properties of yttria stabilized zirconia coatings with CMAS deposits. J Eur Ceram. 2011;31:1881–88.
13. Turcer LR, Padture NP. Rare-earth pyrosilicate solid-solution environmental-barrier coating ceramics for resistance against attack by molten calcia–magnesia–aluminosilicate (CMAS) glass. J Mater Res. 2020;35(17):2373–84.
14. Kim SH, Nagashima N, Matsushita Y, Kim BN, Jang BK. Corrosion behavior of calcium–magnesium–aluminosilicate (CMAS) on sintered Gd_2SiO_5 for environmental barrier coatings. J Am Ceram Soc. 2021;104:3119–29.
15. Wang L, Guo L, Li Z, Peng H, Ma Y, Gong S, et al. Protectiveness of Pt and $Gd_2Zr_2O_7$ layers on EB-PVD YSZ thermal barrier coatings against calcium–magnesium–alumina–silicate (CMAS) attack. Ceram Int. 2015;41:11662–69.
16. Zhou Y, Sun Z. Electronic structure and bonding properties in layered ternary carbide Ti_3SiC_2. J Phys. 2000;12:L457–62.
17. Radovic M, Barsoum MW. MAX phases: bridging the gap between metals and ceramics. Am Ceram Soc Bull. 2013;92(3):20–27.
18. Inoue K, Yamaguchi A. Synthesis of Al_4SiC_4. J Am Ceram Soc. 2003;86:1028–30.
19. Huang XX, Wen GW, Cheng XM, Zhang BY. Oxidation behavior of Al_4SiC_4 ceramic up to 1700°C. Corros Sci. 2007;49:2059–70.
20. Gubarevich AV, Watanabe T, Nishimura T, Yoshida K. Combustion synthesis of single-phase Al_4SiC_4 powder with assistance of induction heating. J Am Ceram Soc. 2020;103:744–49.
21. Wills R, Goodrich S. The oxidation of aluminum silicon carbide. Ceram Eng Sci Proc. 2005;26:181–88.
22. Lee JS, Lee SH, Nishimura T, Tanaka H. Hexagonal platelike ternary carbide particulates synthesized by a carbothermal reduction process: processing parameters and synthesis mechanism. J Am Ceram Soc. 2009;92:1030–35.
23. Lee JS, Lee SH, Nishimura T, Hirosaki N, Tanaka H. A ternary compound additive for vacuum densification of β-silicon carbide at low temperature. J Euro Ceram Soc. 2009;29:3419–23.
24. Inoue K, Yamaguchi A, Hashimoto S. Fabrication and oxidation resistance of Al_4SiC_4 body. J Ceram Soc Japan. 2002;110:1010–15. (in Japanese)
25. Tanaka A, Gubarevich A, Nishimura T, Yoshida K. Oxidation behavior of Al_4SiC_4-based ceramics at 1623K. Energy Rep. in print.
26. Padture NP. Advanced structural ceramics in aerospace propulsion. Nat Mater. 2016;15:804–9.
27. Riley FL. 4 Silicon carbide. Structural ceramics fundamentals and case studies. New York, NY: Cambridge University Press; 2009.
28. Sun Y, Nie X, Cai C, Yang L, Zhou Y. Phase transformation failure in YSZ TBCs induced by component-dependent CMAS corrosion. Surf Coat Technol. 2023;464:129547
29. Levi CG, Hutchinson JW, Vidal-Sétif MH, Johnson CA. Environmental degradation of thermal-barrier coatings by molten deposits. MRS Bull. 2012;37:932–41.
30. Osborn EF, Tait DB. The system diopside-forsterite-anorthite. Am J Sci. 1952;Bowen:751–88.
31. Yamamoto O, Ohtani M, Sasamoto T. Preparation and oxidation of Al_4SiC_4, J Mater Res. 2002;17(4):774–78.

32. Heimann RB, Maggetti M. The struggle between thermodynamics and kinetics: phase evolution of ancient and historical ceramics. In: Artioli G, Oberti R, editors. EMU notes in mineralogy. London: EMU and MSGBI; 2019:233–81.

SUPPORTING INFORMATION

Additional supporting information can be found online in the Supporting Information section at the end of this article.

How to cite this article: Tanaka A, Gubarevich A, Nishimura T, Yoshida K. Corrosion behavior of Al_4SiC_4/SiC ceramics exposed to molten calcium-magnesium-alumino-silicate at 1350°C in air. Int J Appl Ceram Technol. 2024;1–12. https://doi.org/10.1111/ijac.14760